Reversible σ-Bond Formation in Bowl-Shaped π-Radical Cations: The Effects of Curved and Planar Structures

Hiroki Yokoi, Satoru Hiroto,* and Hiroshi Shinokubo*

Department of Molecular and Macromolecular Chemistry, Graduate School of Engineering, Nagoya University, Nagoya, Aichi 464-8603, Japan.

ABSTRACT: The reversible formation of σ-bonds between organic radicals has been widely investigated. However, reports on the formation of σ-dimers from delocalized π-radical cations are scarce. Herein, we report the reversible σ-dimerization behavior of a bowl-shaped π-radical cation generated from a nitrogen-embedded buckybowl, both in the crystalline state and in solution. The detailed structure of the σ-dimer in the crystalline state was determined by a single-crystal X-ray diffraction analysis. The monomeric radical cation exists predominantly in solution at room temperature, while dimerization of the radical cations occurs through carbon–carbon σ-bond formation upon reducing the temperature. ^{1}H NMR and optical spectroscopy measurements confirmed the formation of a σ-dimer at low temperature. Comparative studies with a similar yet planar π-conjugated system suggested that the curved structure of the bowl-shaped π-radical cation facilitates the σ-dimerization at one of the internal sp^2–hybridized carbon atoms. This trend was also observed for the nucleophilic addition reaction of methanol to the π-radical cations. The methoxylation reaction proceeded only for the curved π-radical cation. Theoretical calculations revealed that the large relief of structural strain at the α-carbon atom during the dimerization or nucleophilic addition reactions accelerated the bond formation at the internal carbon atom of the curved radical cation.

Introduction

Reversible σ-bond formation and dissociation processes of organic radicals have attracted great attention in the fields of polymeric soft matter, self-healing, and mechanochromic materials.[1-3] However, among these studies, examples for the reversible σ-dimerization of radical cations remain limited due to the coulombic repulsion between the two positively charged species and/or the instability of the monomeric radical cations. Furthermore, delocalized π-conjugated radical cations usually form π-dimers both in solution and the solid state.

A σ-bonded dicationic dimer has been proposed as the key intermediate in oxidative C–C-bond-forming reactions such as the electrochemical polymerization of thiophenes or pyrroles.[4] However, direct observations of these dicationic species have remained challenging on account of their generally short lifetimes. To date, several research groups have succeeded in the observation of such σ-dimeric dications.[5] For example, Effenberger and co-workers have reported the oxidative dimerization of amino-substituted benzene derivatives and elucidated the structure of the σ-bonded dicationic dimer by single-crystal X-ray diffraction analysis.[5b-e] Merz and co-workers have revealed that the interconversion between σ-dicationic species that consist of two bipyrroles and the corresponding monomers proceeds reversibly in solution depending on the temperature.[5g] Power and co-workers have demonstrated the σ-dimerization of persistent organic radical cations in the crystalline state.[5m] However, their low solubility hampered detailed studies in solution. Therefore, examples for organic radical cations that generate σ-bonded dimers both in the crystalline state and in solution remain so far elusive.

Most reactions of π-conjugated molecules occur at the peripheral positions rather than at the internal atoms. For instance, all reversible σ-dimerization reactions of organic radical cations occur at their peripheral carbon atoms. On the other hand, in the case of nanocarbon materials such as fullerenes, carbon nanotubes, and graphene, reactions can proceed at the internal sp^2 carbon atoms on the surface.[6,7] Recently, such a specific reactivity has also been reported for bowl-shaped π-conjugated molecules.[8] While the reactions of corannulene usually proceed at the peripheral sp^2 carbon atoms, the addition of dihalocarbene to corannulene occurs at its internal sp^2 carbon atom.[8a] Petrukhina and co-workers succeeded in the isolation and characterization of inner-substituted corannulene arenium cations.[8b] In 2008, Scott and Bronstein carried out theoretical calculations, which suggested the relief of geometric strain during addition reactions at internal sp^2 carbons is larger in bowl-shaped molecules than in planar π-systems.[8h] However, no report has experimentally demonstrated the effect of a curved π-structure on the specific reactivity at the internal position through a comparative study with a planar analogue.

Recently, Nozaki and co-wokers and our group have independently succeeded in the synthesis of penta-*peri*-pentabenzoazacorannulene **1** as a buckybowl with a nitrogen atom at its center.[9] We found that oxidation of **1** with tris(4-bromophenyl)ammoniumyl hexachloroantimonate (BAHA) successfully afforded the radical cation $\mathbf{1}^{\bullet+}[SbCl_6]^-$ due to its electron-rich nature (Scheme 1). The persistent nature of this radical cation has enabled a detailed investigation of its chemical properties. Herein, we disclose the reversible σ-bond formation behavior of $\mathbf{1}^{\bullet+}$ at an internal sp^2 carbon atom by crystallization or lowering the

temperature of its solution. We also experimentally demonstrate the importance of the curved structure for the σ-dimerization through comparison with an analogous planar radical cation, $\mathbf{2}^{\bullet+}[SbCl_6]^-$, which in contrast undergoes selective π-dimerization.

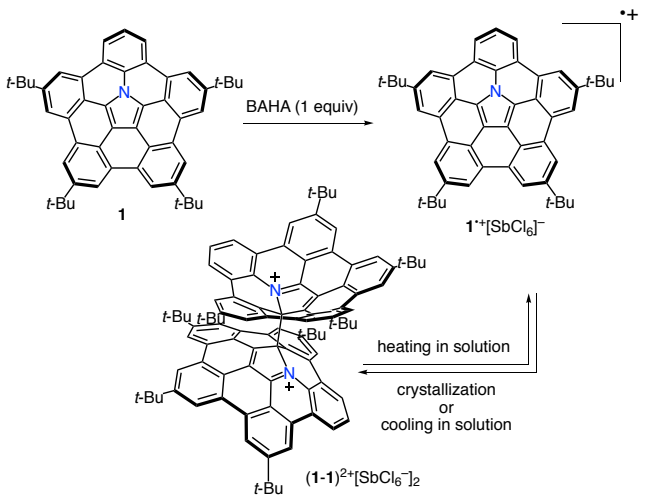

Scheme 1. Dimerization and dissociation behavior of $\mathbf{1}^{\bullet+}[SbCl_6]^-$ and $(\mathbf{1}\text{-}\mathbf{1})^{2+}[SbCl_6^-]_2$.

Results and Discussion

σ-Dimerization of the bowl-shaped radical cation.

To characterize the detailed structure of $\mathbf{1}^{\bullet+}$, we attempted to obtain single crystals by vapor diffusion of hexane into a chlorobenzene/diethyl ether solution of $\mathbf{1}^{\bullet+}[SbCl_6]^-$. Contrary to our expectations, we obtained the crystal of σ-dimer $(\mathbf{1}\text{-}\mathbf{1})^{2+}[SbCl_6^-]_2$, wherein two azabuckybowl units are connected by a covalent carbon–carbon bond between the internal α-carbons of the central pyrrole rings (Figure 1).[10,11] The sum of the angles around the α-carbons (326°/327°) clearly indicates a sp^3 hybridization. In addition, the existence of two counter-anions in the unit cell indicates a dicationic nature of this dimer. The length of the central bridging bond (1.641(5) Å) is close to those of previously reported σ-dimeric dications (1.637(5) Å),[5m] but obviously longer than standard $C(sp^3)$–$C(sp^3)$ single bonds (1.54 Å). As reported previously, $\mathbf{1}^{\bullet+}[SbCl_6]^-$ exists as a monomer in solution at room temperature, and consequently, the dimerization of $\mathbf{1}^{\bullet+}$ should be induced by crystallization. In fact, dissolution of the crystal of the σ-dimer in CH_2Cl_2 regenerated the monomeric radical cation $\mathbf{1}^{\bullet+}$ (Figure S6).

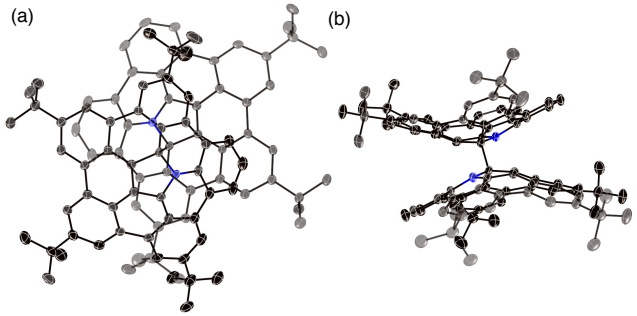

Figure 1. X-ray crystal structure of $(\mathbf{1}\text{-}\mathbf{1})^{2+}[SbCl_6^-]_2$. (a) Top view and (b) side view. Thermal ellipsoids are set at 50% probability, and all hydrogen atoms, solvent molecules, and $[SbCl_6]^-$ ions have been omitted for clarity.

The σ-dimerization reaction was also observed in solution upon lowering the temperature. Figure 2a shows the variable-temperature (VT) ^1H NMR spectra of $\mathbf{1}^{\bullet+}[SbCl_6]^-$ in $CDCl_3$. No signal was observed at 25 °C, suggesting the predominant existence of a paramagnetic species at room temperature. Broad peaks gradually appeared in the aromatic region with decreasing temperature. These peaks finally became sharp at –55 °C, indicating the formation of a diamagnetic species. Based on ^1H–^1H correlation spectroscopy (COSY) NMR measurements and the relative integral values estimated by comparison with those of tris(4-bromophenyl)amine, eight singlets, two doublets, and one triplet were identified in the spectrum (Figure S7 and S8). These signals were assigned to the peripheral protons of a penta-*peri*-pentabenzoazacorannulene with low symmetry.

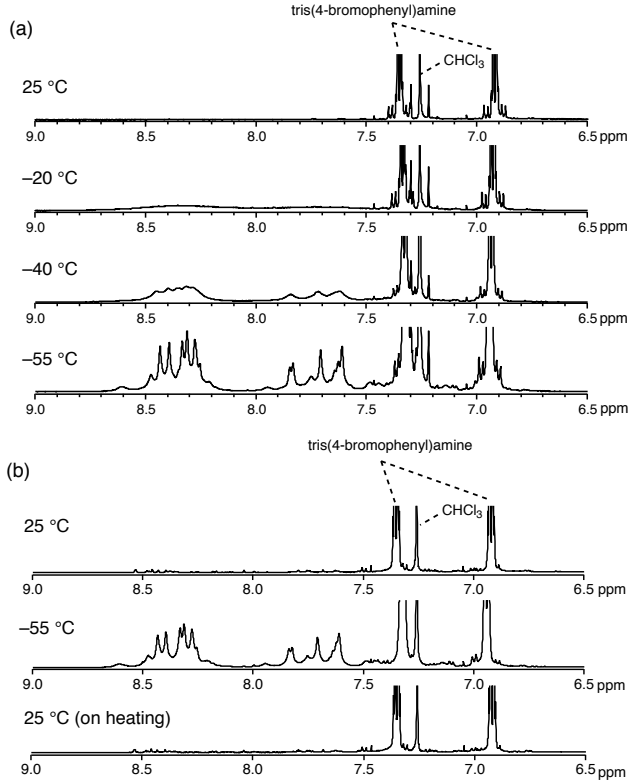

Figure 2. Variable-temperature ^1H NMR spectra of $\mathbf{1}^{\bullet+}[SbCl_6]^-$ (a) on cooling from 25 °C (top) to –55 °C (bottom) in $CDCl_3$ and (b) on cooling from 25 °C (top) to –55 °C (middle) and heating from –55°C to 25 °C (bottom) in $CDCl_3$.

We also measured the VT UV-vis-NIR absorption spectra of $\mathbf{1}^{\bullet+}[SbCl_6]^-$ in CH_2Cl_2 (Figure 3a). At room temperature, a characteristic broad band in the near-infrared (NIR) region was observed, which was assigned to the monomeric radical cation. In contrast, the intensity of this NIR absorption band decreased at lower temperatures, while new absorption bands at around 580 and 720 nm appeared with isosbestic points. The disappearance of the NIR absorption band suggests the formation of a σ-dimer.[5g,i] In addition, the simulated absorption spectrum of the σ-dimer $(\mathbf{1}\text{-}\mathbf{1})^{2+}$ calculated by a time-dependent (TD) DFT method is in good agreement with the experimental spectrum (Figure S9). These spectroscopic analyses suggest the formation of the σ-dimer $(\mathbf{1}\text{-}\mathbf{1})^{2+}$ in solution and in the crystalline state. Upon heating the once-cooled solution, both ^1H NMR and the absorption spectra were reverted to those for the monomeric radical cation $\mathbf{1}^{\bullet+}$ (Figure 2b and 3b). Thus, the

dimerization and dissociation are reversible in solution depending on temperatures. According to the optical experiments, the thermodynamic parameters of this dimerization process were determined to be ΔH = –11.1 kcal mol^{-1} and ΔS = –30.2 cal K^{-1} mol^{-1} by means of a van't Hoff plot (Figure S10). We also performed VT ESR measurements in CH_2Cl_2 (Figure 4). The signal derived from **1**$^{\bullet+}$ completely disappeared at –85 °C. Based on these experiments, the thermodynamic parameters were estimated to be ΔH = –11.8 kcal mol^{-1} and ΔS = –28.5 cal K^{-1} mol^{-1}, i.e., they are similar to those determined by optical measurements (Figure S11). The ΔH value for this system is higher than that of previously reported σ-dimeric dications.[5i–k] Furthermore, the dimerizations of alkylated C_{60} radicals exhibit much smaller ΔH values (up to –35.5 kcal mol^{-1}).[12] The crystal of σ-dimer easily dissociates to regenerate the corresponding monomers in solution, consisting with the relatively high ΔH value of **1**$^{\bullet+}$.

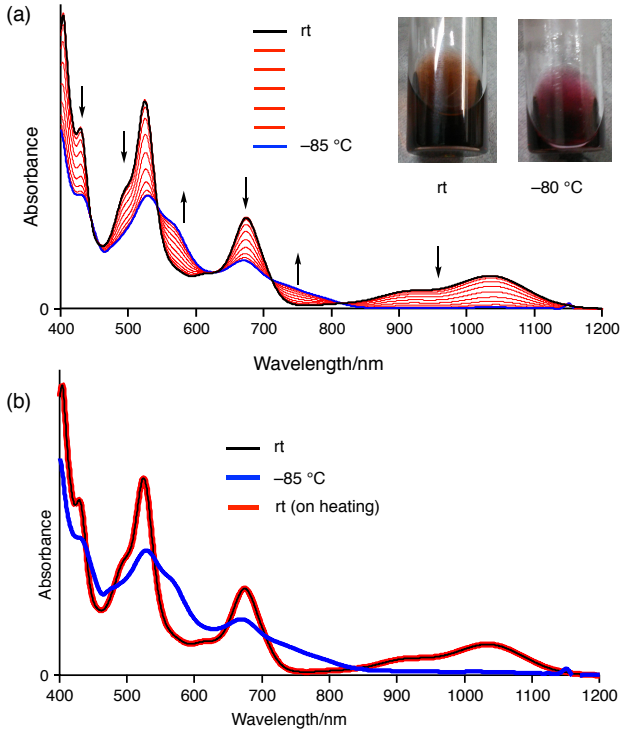

Figure 3. Variable-temperature UV-vis-NIR absorption spectra of **1**$^{\bullet+}$[$SbCl_6$]$^-$ in CH_2Cl_2 (a) on cooling and (b) on heating the once-cooled solution. The inset shows the change of the solution color.

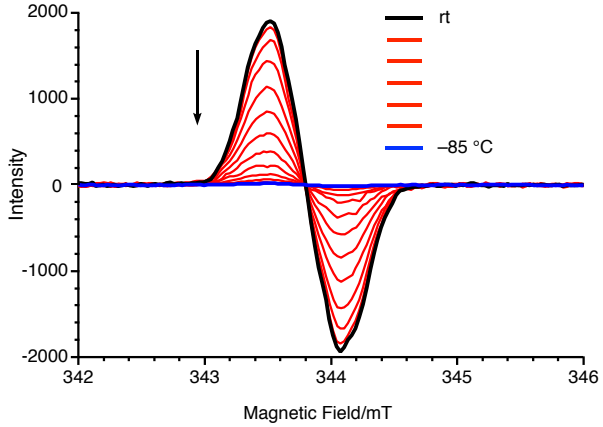

Figure 4. Variable-temperature ESR spectra of **1**$^{\bullet+}$[$SbCl_6$]$^-$ in CH_2Cl_2.

π-Dimerization of an analogous planar radical cation.

In contrast to the behavior of the present bowl-shaped π-radical cation **1**$^{\bullet+}$, delocalized π-radical cations often form π-dimers in solution.[13] We envisioned that the bowl-shaped structure of **1**$^{\bullet+}$ contributes to the formation of a σ-bond at an internal position. To elucidate the effect of bowl shape on the σ-dimerization, we prepared the analogous planar molecule **2** (Scheme 2). The structure of **2** is, except for one less carbon–carbon bond, identical to that of **1**. The detailed structure of **2** was unambiguously elucidated by a single-crystal X-ray diffraction analysis. In the crystal, four independent molecules are arranged to form a 1D columnar π-stack (Figure S12).[14] Deviations from the mean plane formed by the 35 core atoms are 0.077 Å, 0.125 Å, 0.135 Å, and 0.154 Å, which corroborate the presence of a highly planar structure.

With the planar analogue **2** in hand, we conducted comparison experiments. The oxidation of **2** with 1 equiv of BAHA resulted in the disappearance of its ^{1}H NMR signals under concomitant emergence of NIR bands in the UV-vis-NIR absorption spectrum (Figure S13 and S14). The formation of a paramagnetic species was confirmed by ESR measurements in CH_2Cl_2 solution, which showed a distinct peak at g = 2.003 (Figure S15). The simulated UV-vis-NIR absorption spectrum of **2**$^{\bullet+}$ by TD-DFT calculations at the B3LYP/6-31G(d) level of theory was consistent with the experimental results, supporting the formation of **2**$^{\bullet+}$ (Figure S16). Fortunately, we obtained the X-ray crystal structure of **2**$^{\bullet+}$, which revealed that the radical cation structure remains nearly planar (Figure 5).[15] The mean plane deviation became 0.131 Å, which is almost identical to the averaged deviation value for **2** (0.123 Å). Furthermore, in the crystal, two molecules of **2**$^{\bullet+}$ were found to be stacked in a face-to-face manner. The presence of 2 equiv of the counter anion [$SbCl_6$]$^-$ in one unit cell confirmed the dicationic character of this dimer. The closest interplanar distance (3.14 (1) Å), which is a typical value for π-dimers, was observed between the two α-carbon atoms of the central pyrrole rings.[13a-d,16] Such a shorter distance than the sum of the van der Waals radii of two C(sp^2) atoms (3.40 Å) indicates the presence of strong attractive interactions between these two paramagnetic species.[17]

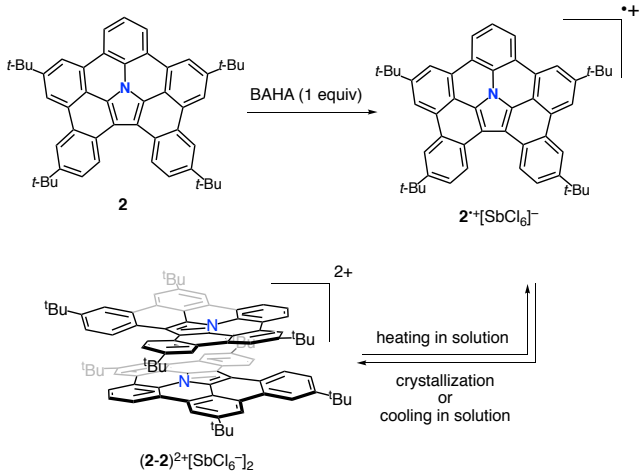

Scheme 2. Dimerization and dissociation behavior of **2**$^{\bullet+}$[$SbCl_6$]$^-$ and (**2**-**2**)$^{2+}$[$SbCl_6^-$]$_2$.

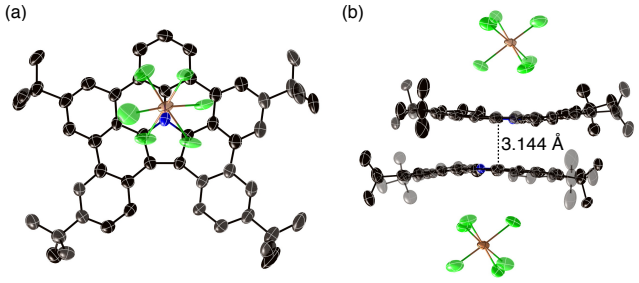

Figure 5. X-ray crystal structure of $(\mathbf{2}\text{-}\mathbf{2})^{2+}[SbCl_6^-]_2$. (a) Top view and (b) packing structure. Thermal ellipsoids set at 50% probability; all hydrogen atoms and solvent molecules have been omitted for clarity.

The dimerization behavior of $\mathbf{2}^{\bullet+}$ in solution was investigated. In the VT ^{1}H NMR measurements, two broad peaks were observed in the aromatic region at –80 °C, indicating the existence of a diamagnetic species (Figure 6). These changes were also monitored by VT ESR spectroscopy. The intensity of the single peak at g = 2.003 corresponding to $\mathbf{2}^{\bullet+}$ gradually weakened at low temperatures (Figure S17). In contrast to the case of $\mathbf{1}^{\bullet+}$, the signal was still observed at –85 °C. The structure of the resulting product was finally determined by the VT UV-vis-NIR absorption analysis of $\mathbf{2}^{\bullet+}$ (Figure 7a). The absorption bands in the UV-vis region remained almost unchanged at low temperatures. On the other hand, a new absorption band appeared at ~1300 nm. According to reported π-dimerization reactions, the appearance of a NIR absorption band at low temperatures strongly suggests the formation of a π-dimer. TD-DFT calculations on the π-dimer $(\mathbf{1}\text{-}\mathbf{1})^{2+}$ also supported the observed spectral changes (Figure S18). The new absorption band at ~1300 nm was mostly attributed to the transition from the HOMO–1 to the LUMO of the π-dimer. Regarding the HOMO–1, bonding interactions were found between the two units of $\mathbf{2}^{\bullet+}$ (Figure S19). Consequently, the appearance of this band suggests the formation of a π-dimer. According to Figure 7b, the dimerization of $\mathbf{2}^{\bullet+}$ proceeds reversibly in solution depending on temperatures. The thermodynamic parameters were determined to be ΔH = –5.8 kcal mol^{-1} and ΔS = –11.0 cal K^{-1} mol^{-1} by ESR measurements (Figure S20). The ΔH value is much smaller than that for the σ-dimerization of $\mathbf{1}^{\bullet+}$.

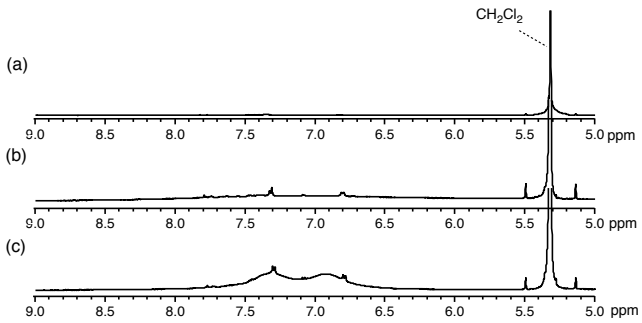

Figure 6. Variable-temperature ^{1}H NMR spectra of $\mathbf{2}^{\bullet+}[SbCl_6]^-$ in CD_2Cl_2 at (a) 25 °C, (b) –40 °C, and (c) –80 °C.

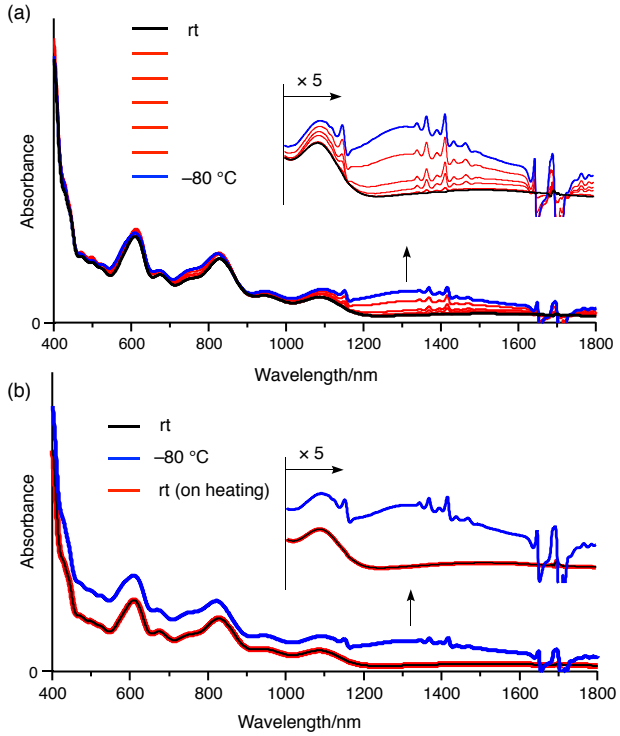

Figure 7. Variable-temperature UV-vis-NIR absorption spectra of $\mathbf{2}^{\bullet+}[SbCl_6]^-$ in CH_2Cl_2 (a) on cooling and (b) on heating the once-cooled solution.

Nucleophilic additions to the bowl-shaped radical cations.

The specific reactivity at the internal carbon atom of $\mathbf{1}^{\bullet+}$ is also reflected in its reaction with nucleophiles. In the presence of an excess of methanol, $\mathbf{1}^{\bullet+}$ was converted into methoxylated $(\mathbf{1}\bullet\mathbf{OMe})^+$ in 99% yield, whereas no reaction occurred in the case of $\mathbf{2}^{\bullet+}$ (Figure S21). In the ^{1}H NMR spectrum of $(\mathbf{1}\bullet\mathbf{OMe})^+$ in $CDCl_3$, eight singlets, two doublets, and one triplet were observed in the aromatic region, consistent with a structure of lower symmetry. The X-ray crystal structure of $(\mathbf{1}\bullet\mathbf{OMe})^+$ revealed that the methoxy group was introduced selectively at the α-carbon atom of the central pyrrole ring (Figure 8).[18] The length of the C1–O1 bond (1.417(3) Å) is consistent with a standard C–O single bond (1.43 Å), while the C2–C3 bond length (1.359(4) Å) suggests double bond character. In addition, the N1–C4 bond (1.337(3) Å) is longer than typical C–N double bonds (1.28 Å), but shorter than C–N single bonds (1.47 Å). Accordingly, $(\mathbf{1}\bullet\mathbf{OMe})^+$ presents a large contribution of the resonance structures depicted in Figure 8c. Interestingly, only 1 equiv of BAHA was required to complete the generation of $(\mathbf{1}\bullet\mathbf{OMe})^+$ from **1**. This addition reaction should be initiated by the nucleophilic attack of methanol to the α-carbon atom of the central pyrrole ring (Scheme 3).[19] A subsequent deprotonation would result in the formation of neutral radical $(\mathbf{1}\bullet\mathbf{OMe})^{\bullet}$. Considering that the hexachloroantimonate ion can serve as an oxidant, $(\mathbf{1}\bullet\mathbf{OMe})^{\bullet}$ may be oxidized to afford $(\mathbf{1}\bullet\mathbf{OMe})^+$.[20] The change of oxidizing agent from BAHA to $Ag[PF_6]$, where the hexafluorophosphate ion has no oxidizing ability, resulted in a decrease of the yield to 63% (Figure S22). Figure 9 shows the UV-vis absorption spectrum of $(\mathbf{1}\bullet\mathbf{OMe})^+$ in CH_2Cl_2, which exhibits two characteristic absorption bands in the visible region. The spectral similarity between $(\mathbf{1}\bullet\mathbf{OMe})^+$ and σ-dimer $(\mathbf{1}\text{-}\mathbf{1})^{2+}$ demonstrates the resemblance of the electronic structures of these two cationic species.

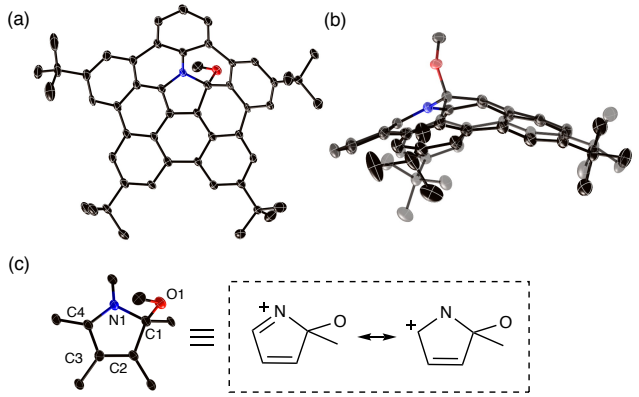

Figure 8. X-ray crystal structure of $(\mathbf{1}\bullet\mathbf{OMe})^{+}[SbCl_6]^{-}$. (a) Top view and (b) side view. Thermal ellipsoids set at 50% probability; all hydrogen atoms, the $[SbCl_6]^{-}$ ion, and solvent molecules have been omitted for clarity; selected bond lengths [Å]: N1–C1 1.487(3), C1–C2 1.499(4), C2–C3 1.359(4), C3–C4 1.412(4), C4–N1 1.337(3), C1–O1 1.417(3).

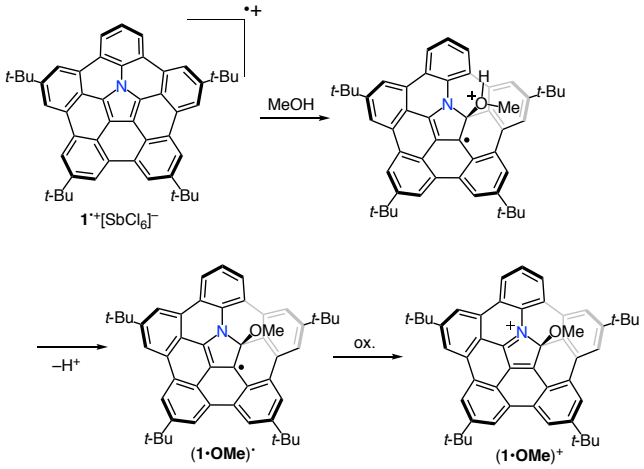

Scheme 3. Proposed reaction mechanism for the methoxylation of $\mathbf{1}^{\bullet+}[SbCl_6]^{-}$.

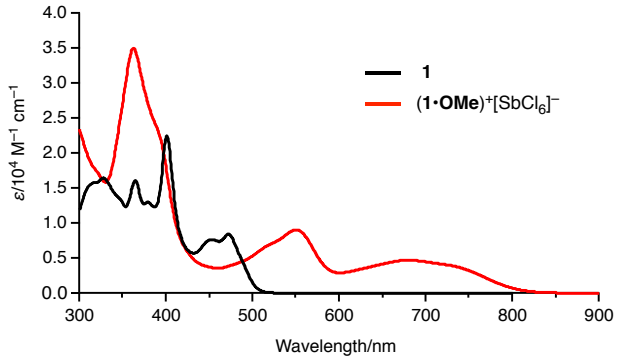

Figure 9. UV-vis absorption spectra of **1** and $(\mathbf{1}\bullet\mathbf{OMe})^{+}[SbCl_6]^{-}$ in CH_2Cl_2.

Origin of the distinct reactivity of the bowl-shaped radical cation

For bowl-shaped π-conjugated molecules such as corannulene and sumanene, the pyramidalization strain mainly concentrates on the internal sp^2 carbon atoms rather than in the peripheral region.[21,22] Consequently, the major driving force for the chemical reaction at internal positions should be a large relief of strain. We carried out DFT calculations of the electronic and geometric structures of $\mathbf{1}^{\bullet+}$ and $\mathbf{2}^{\bullet+}$ at the B3LYP/6-31G(d) level of theory (Figure 10). For both radical cations, the spin density is mostly located on the α-carbon atom of the central pyrrole ring. The spin density at this position is almost the same for both radical cations, indicating that their electronic character is not the origin of their different reactivity. We also estimated the π-orbital axis vector (POAV) angles, which indicate the degree of curvature.[23] As expected, $\mathbf{1}^{\bullet+}$ exhibits a relatively large POAV angle at its internal α-carbon atom ($\theta_{\sigma\pi}$ = 6.6°). On the other hand, $\mathbf{2}^{\bullet+}$ exhibits a planar structure, which results in a significantly smaller POAV angle ($\theta_{\sigma\pi}$ = 0.5°). In the σ-dimer $(\mathbf{1}\text{-}\mathbf{1})^{2+}$ and the methoxylated product $(\mathbf{1}\bullet\mathbf{OMe})^{+}$, the POAV angles of the newly formed sp^3 carbon atoms are close to the ideal sp^3 geometry ($\theta_{\sigma\pi}$ = 20.0° and 21.5°, respectively) (Figure S23), which means that the geometric strain at these positions has been successfully relieved. On the other hand, the POAV angles of the other sp^2 carbon atoms in the central pyrrole ring became slightly smaller than those of $\mathbf{1}^{\bullet+}$. Thus, the dimerization and methoxylation leads to an additional relief of the pyramidalization strain at the remaining sp^2 carbon atoms.

Finally, we carried out DFT calculations of the homodesmotic reaction shown in Scheme 4 in order to estimate the relative energy balance during the course of the methoxylation. The addition reaction of $\mathbf{1}^{\bullet+}$ was determined to be by 15.2 kcal mol^{-1} energetically more favorable than that of $\mathbf{2}^{\bullet+}$ (Table S2). These results clearly indicate that the release of strain is higher in $\mathbf{1}^{\bullet+}$ than in $\mathbf{2}^{\bullet+}$, thus accelerating the bond formation at the internal position of $\mathbf{1}^{\bullet+}$. In contrast, the addition reaction of $\mathbf{2}^{\bullet+}$ increases the geometric strain at the newly formed sp^3 carbon atom and the neighboring atoms.

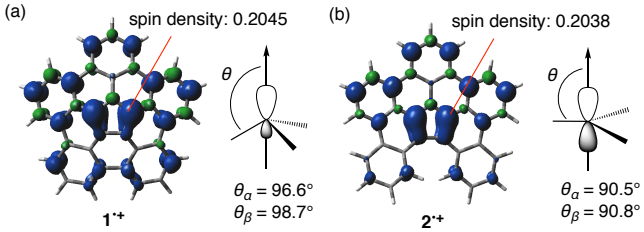

Figure 10. POAV angles and spin-density distribution of (a) $\mathbf{1}^{\bullet+}$ and (b) $\mathbf{2}^{\bullet+}$, calculated at the B3LYP/6-31G(d) level of theory; *tert*-butyl substituents were replaced by hydrogen atoms.

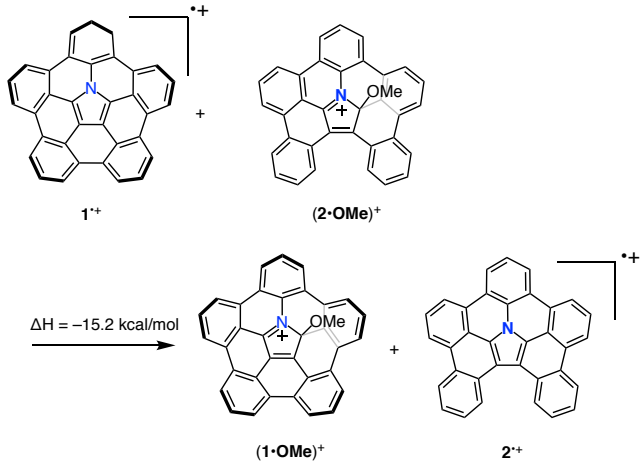

Scheme 4. Energy for the homodesmotic reaction, calculated at the B3LYP/6-31G(d) level of theory; *tert*-butyl substituents were replaced by hydrogen atoms.

Conclusion

We have investigated the unique dimerization behavior of a radical cation with a bowl-shaped structure. In the crystalline state, $\mathbf{1}^{\bullet+}$ affords a σ-dimeric dication, where bond formation occurs between the internal α-carbon atoms of the central pyrrole rings. Different from many other organic radical cations, $\mathbf{1}^{\bullet+}$ exhibits reversible temperature-dependent σ-dimerization behavior in solution. The formation of the σ-dimer is dominant at low temperatures, suggesting that the dimer is thermodynamically more stable than the monomer. In sharp contrast, planar radical cation $\mathbf{2}^{\bullet+}$ furnishes selectively a π-dimer both in the crystalline state and in solution. A different reactivity for $\mathbf{1}^{\bullet+}$ and $\mathbf{2}^{\bullet+}$ was also observed with respect to their nucleophilic addition reaction with methanol. The bowl-shaped radical cation $\mathbf{1}^{\bullet+}$ reacted with methanol to form an α-methoxylated product, while no changes were observed in the case of the planar radical cation $\mathbf{2}^{\bullet+}$. The bowl-shaped structure is advantageous for bond formation at the internal curved surface due to the resulting large relief of the pyramidalization strain. On the other hand, the addition reaction to the internal sp^2 carbon atoms of the planar π-system is energetically unfavorable due to the conversion of a trigonal planar sp^2 carbon atom into a tetrahedral sp^3 carbon atom, which increases the geometric strain. These hypotheses were supported by theoretical calculations. The reactivity of $\mathbf{1}^{\bullet+}$ is analogous to the chemistry of aza[60]fullerene radical $C_{59}N^{\bullet}$, which forms a σ-dimer $(C_{59}N)_2$ and reacts with nucleophiles at the carbon atoms adjacent to the nitrogen atom.[24] This fact promises that **1** should be a good model for aza[60]fullerene. Our research offers new insights into the molecular design of advanced materials by exploiting the reversible σ-dimerization behavior of organic radical cations.

ASSOCIATED CONTENT

Supporting Information

Experimental procedures and spectroscopic data, X-ray data, and the results of theoretical calculations. This material is available free of charge via the Internet at http://pubs.acs.org.

AUTHOR INFORMATION

Corresponding Author

* hiroto@chembio.nagoya-u.ac.jp;
hshino@chembio.nagoya-u.ac.jp

ACKNOWLEDGMENT

We would like to acknowledge Prof. Taishi Takenobu and Dr. Hisaaki Tanaka (Nagoya University) for their help with the VT ESR measurements. This work was supported by JSPS KAKENHI grants JP16H06031, JP26102003, and JP15H00731, as well as the Program for Leading Graduate Schools "Integrative Graduate Education and Research in Green Natural Sciences" from MEXT (Japan). S. H. expresses his gratitude for the financial support from the Tokuyama Science Foundation. Y. H. acknowledges a grant-in-aid for JSPS Research Fellows (JP15J10528).

REFERENCES

(1) Zafra, J. L.; Qiu, L.; Yanai, N.; Mori, T.; Nakano, M.; Alvarez, M. P.; López Navarrete, J. T.; Gómez-García, C. J.; Kertesz, M.; Takimiya, K.; Casado, J. *Angew. Chem. Int. Ed.* **2016**, *55*, 14563.

(2) (a) Imato, K.; Takahara, A.; Otsuka, H. *Macromolecules* **2015**, *48*, 5632. (b) Imato, K.; Nishihara, M.; Kanehara, T.; Amamoto, Y.; Takahara, A.; Otsuka, H. *Angew. Chem. Int. Ed.* **2012**, *51*, 1138.

(3) (a) Wang, Y.; Tan, X.; Zhang, Y.-M.; Zhu, S.; Zhang, I.; Yu, B.; Wang, K.; Yang, B.; Li, M.; Zou, B.; Zhang, S. X.-A. *J. Am. Chem. Soc.* **2015**, *137*, 931. (b) Ruiz de Luzuriaga, A.; Matxain, J. M.; Ruipérez, F.; Martin, R.; Asua, J. M.; Cabañero, G.; Odriozola, I. *J. Mater. Chem. C* **2016**, *4*, 6220. (c) Imato, K.; Natterodt, J. C.; Sapkota, J.; Goseki, R.; Weder, C.; Takahara, A.; Otsuka, H. *Polym. Chem.* **2017**, *8*, 2115.

(4) (a) Heinze, J.; Frontana-Uribe, B. A.; Ludwigs, S. *Chem. Rev.* **2010**, *110*, 4724. (b) Seo, E. T.; Nelson, R. F.; Fritsch, J. M.; Marcoux, L. S.; Leedy, D. W.; Adams, R. N. *J. Am. Chem. Soc.* **1966**, *88*, 3498. (c) Creason, S. C.; Wheeler, J.; Nelson, R. F. *J. Org. Chem.* **1972**, *37*, 4440.

(5) (a) Nishinaga, T.; Komatsu, K. *Org. Biomol. Chem.* **2005**, *3*, 561. (b) Effenberger, F.; Stohrer, W. D.; Steinbach, A. *Angew. Chem. Int. Ed. Engl.* **1969**, *8*, 280. (c) Effenberger, F.; Mack, K. E.; Niess, R.; Reisinger, F.; Steinbach, A.; Stohrer, W. D.; Stezowski, J. J.; Rommel, I.; Maier, A. *J. Org. Chem.* **1988**, *53*, 4379. (d) Effenberger, F. *Acc. Chem. Res.* **1989**, *22*, 27. (e) Effenberger, F.; Stohrer, W. D.; Mack, K. E.; Reisinger, F.; Seufert, W.; Kramer, H. E. A.; Föll, R.; Vogelmann, E. *J. Am. Chem. Soc.* **1990**, *112*, 4849. (f) Heinze, J.; Willmann, C.; Bäuerle, P. *Angew. Chem. Int. Ed.* **2001**, *40*, 2861. (g) Merz, A.; Kronberger, J.; Dunsch, L.; Neudeck, A.; Petr, A.; Parkanyi, L. *Angew. Chem. Int. Ed.* **1999**, *38*, 1442. (h) Taquet, J.; Siri, O.; Collin, J. P.; Messaoudi, A.; Braunstein, P. *New J. Chem.* **2005**, *29*, 188. (i) Smie, A.; Heinze, J. *Angew. Chem. Int. Ed.* **1997**, *36*, 363. (j) Tschuncky, P.; Heinze, J.; Smie, A.; Engelmann, G. Kossmehl, G. *J. Electroanal. Chem.* **1997**, *433*, 223. (k) Heinze, J.; Tschuncky, P.; Smie, A. *J. Solid State Electrochem.* **1998**, *2*, 102. (l) Heinze, J.; John, H.; Dietrich, M.; Tschuncky, P. *Synth. Met.* **2001**, *119*, 49. (m) Chen, X.; Wang, X.; Zhou, Z.; Li, Y.; Sui, Y.; Ma, J.; Wang, X.; Power, P. P. *Angew. Chem. Int. Ed.* **2013**, *52*, 589.

(6) Hirsch, A.; Brettreich, M. *Fullerenes: Chemistry and Reactions*, Wiley-VCH, Weinheim, **2005**.

(7) (a) Hawkins, J. M.; Meyer, A. *Science* **1993**, *260*, 1918. (b) Balch, A. L.; Catalano, V. J.; Lee, J. W.; Olmstead, M. M.; Parkin, S. R. *J. Am. Chem. Soc.* **1991**, *113*, 8953. (c) Balch, A. L.; Lee, J. W.; Olmstead, M. M. *Angew. Chem. Int. Ed. Engl.* **1992**, *31*, 1356. (d) Hawkins, J. M.; Meyer, A.; Solow, M. A. *J. Am. Chem. Soc.* **1993**, *115*, 7499. (e) Karousis, N.; Tagmatarchis, N. *Chem. Rev.* **2010**, *110*, 5366. (f) Park, J.; Yan, M. *Acc. Chem. Res.* **2013**, *46*, 181.

(8) (a) Preda, D. V.; Scott, L. T. *Tetrahedron Lett.* **2000**, *41*, 9633. (b) Zabula, A. V.; Spisak, S. N.; Filatov, A. S.; Rogachev, A. Yu.; Petrukhina, M. A. *Angew. Chem. Int. Ed.* **2011**, *50*, 2971. (c) Ngamsomprasert, N.; Dang, J.-S.; Higashibayashi, S.; Yakiyama, Y.; Sakurai, H. *Chem. Commun.*, **2017**, *53*, 697. (d) Scott, L. T. *Chem. Soc. Rev.*, **2015**, *44*, 6464. (e) Dubceac, C.; Zabula, A. V.; Filatov, A. S.; Rossi, F.; Zanello, P.; Petrukhina, M. A. *J. Phys. Org. Chem.* **2012**, *25*, 553. (f) Dubceac, C.; Filatov, A. S.; Zabula, A. V.; Petrukhina, M. A. *Cryst. Growth Des.* **2015**, *15*, 778. (g) Yanney, M.; Fronczek, F. R.; Sygula, A. *Org. Lett.* **2012**, *18*, 4942. (h) Bronstein, H. E.; Scott, L. T. *J. Org. Chem.*, **2008**, *73*, 88. (i) Cho, H. Y.; Ansems, R. B. M.; Scott, L. T. *Beilstein J. Org. Chem.* **2014**, *10*, 956.

(9) (a) Yokoi, H.; Hiraoka, Y.; Hiroto, S.; Sakamaki, D.; Seki, S.; Shinokubo, H. *Nat. Commun.* **2015**, *6*, 8215. (b) Ito, S.; Tokimaru, Y.; Nozaki, K. *Angew. Chem. Int. Ed.* **2015**, *54*, 7256.

(10) X-ray crystallographic data for $(\mathbf{1}\text{-}\mathbf{1})^{2+}[SbCl_6^-]_2$: Formula: $C_{106}H_{99}Cl_{13}N_2Sb_2$, M_w = 2105.22, triclinic, space group: *P*-1, a = 17.484(8) Å, b = 18.351(8) Å, c = 18.671(9) Å, α = 110.418(4)°, β = 104.903(2)°, γ = 108.5972(16)°, V = 4842(4) Å^3, Z = 2, D_c = 1.444 g/cm^3, R_1 = 0.0687 ($I > 2\sigma(I)$), wR_2 = 0.2367 (all data), GOF = 1.089. CCDC number: 1815258.

(11) There are two possible diastereomers for $(\mathbf{1}\text{-}\mathbf{1})^{2+}$, a *meso*-dimer and a *chiral* dimer. The calculated energies for the *meso*- and *chiral* dimers are almost identical (see Figure S5 and Table S1); however, only the *meso*-dimer was observed in the crystal structure.

(12) (a) Morton, J. R.; Preston, K. F.; Krusic, P. J.; Wasserman, E. *J. Chem. Soc. Perkin Trans. 2* **1992**, 1425. (b) Morton, J. R.; Preston, K. F. *J. Am. Chem. Soc.* **1992**, *114*, 5454. (c) Lee, Y.; Kitagawa, T.; Komatsu, K. *J. Org. Chem.* **2004**, *69*, 263.

(13) (a) Nishinaga, T.; Komatsu, K. *Org. Biomol. Chem.* **2005**, *3*, 561. (b) Yamazaki, D.; Nishinaga, T.; Tanino, N.; Komatsu, K. *J. Am. Chem. Soc.*

2006, *128*, 14470. (c) Porter, W. W., III; Vaid, T. P. *J. Org. Chem.* **2005**, *70*, 5028. (d) Lü, J.-M.; Rosokha, S. V.; Kochi, J. K. *J. Am. Chem. Soc.* **2003**, *125*, 12161. (e) Graf, D. D.; Duan, R. G.; Campbell, J. P.; Miller, L. L.; Mann, K. R. *J. Am. Chem. Soc.* **1997**, *119*, 5888. (f) Ziganshina, A. Y.; Ko, Y. H.; Jeon, W. S.; Kim, K. *Chem. Commun.* **2004**, 806. (g) Miller, L. L.; Mann, K. R. *Acc. Chem. Res.* **1996**, *29*, 417. (h) Nishinaga, T.; Sotome, Y. *J. Org. Chem.* **2017**, *82*, 7245. (f) Nielsen, C. B.; Angerhofer, A.; Abboud, K. A.; Reynolds, J. R. *J. Am. Chem. Soc.* **2008**, *130*, 9734. (i) Rizalman, N. S.; Ferrón, C. C.; Niu, W.; Wallace, A. L.; He, M.; Balster, R.; Lampkin, J.; Hernández, V.; López Navarrete, J. T.; Ruiz Delgado, M. C.; Hartl, F. *RSC Adv.* **2013**, *3*, 25644.

(14) X-ray crystallographic data for **2**: Formula: $C_{199.77}H_{195.32}N_4$, M_w = 2652.15, monoclinic, space group: $P2_1/n$, a = 21.4102(5) Å, b = 30.3917(5) Å, c = 25.3832(5) Å, β = 108.985(3)°, V = 15618.2(6) Å^3, Z = 4, D_c = 1.128 g/cm^3, R_1 = 0.0607 ($I > 2\,\sigma(I)$), wR_2 = 0.1795 (all data), GOF = 1.033. CCDC number: 1815712.

(15) X-ray crystallographic data for $\mathbf{2}^{\bullet+}$: Formula: $C_{51.83}H_{52.66}Cl_{9.72}NSb_{0.98}$, M_w = 1153.46, monoclinic, space group: $P2_1/c$, a = 11.5521(6) Å, b = 24.1457(9) Å, c = 19.7738(10) Å, β = 106.010(5)°, V = 5301.6(5) Å^3, Z = 4, D_c = 1.445 g/cm^3, R_1 = 0.0945 ($I > 2\,\sigma(I)$), wR_2 = 0.2635 (all data), GOF = 1.083. CCDC number: 1815259.

(16) (a) Femoni, C.; Iapalucci, M. C.; Longoni, G.; Tiozzo, C.; Wolowska, J.; Zacchini, S.; Zazzaroni, E. *Chem.-Eur. J.* **2007**, *13*, 6544. (b) Goto, K.; Kubo, T.; Yamamoto, K.; Nakasuji, K.; Sato, K.; Shiomi, D.; Takui, T.; Kubota, M.; Kobayashi, T.; Yakusi, K.; Ouyang, J. *J. Am. Chem. Soc.* **1999**, *121*, 1619. (c) Merz, A.; Kronberger, J.; Dunsch, L.; Neudeck, A.; Petr, A.; Parkanyi, L. *Angew. Chem. Int. Ed.* **1999**, *38*, 1442.

(17) (a) Preuss, K. E. *Polyhedron* **2014**, *79*, 1. (b) Mota, F.; Miller, J. S.; Novoa, J. J. *J. Am. Chem. Soc.* **2009**, *131*, 7699. (c) Cui, Z.-h.; Lischka, H.; Beneberu, H. Z.; Kertesz, M. *J. Am. Chem. Soc.* **2014**, *136*, 5539.

(18) X-ray crystallographic data for $(\mathbf{1{\bullet}OMe})^+[SbCl_6]^-$: Formula: $C_{128.75}H_{137.16}Cl_{14.90}N_2O_{2.73}Sb_2$, M_w = 2527.94, monoclinic, space group: $C2/c$, a = 32.3774(8) Å, b = 12.2907(3) Å, c = 29.9008(7) Å, β = 90.309(2)°, V = 11898.6(5) Å^3, Z = 4, D_c = 1.411 g/cm^3, R_1 = 0.0541 ($I > 2\,\sigma(I)$), wR_2 = 0.1430 (all data), GOF = 1.081. CCDC number: 1815260.

(19) Adams, C.; Jacobsen, N.; Utley, J. H. P. *J. Chem. Soc. Perkin Trans. 2* **1978**, 1071.

(20) (a) Connelly, N. G.; Geiger, W. E. *Chem. Rev.* **1996**, *96*, 877. (b) Cowell, G. W.; Ledwith, A.; White, A. C.; Woods, H. J. *J. Chem. Soc. B* **1970**, 227.

(21) Petrukhina, M. A. & Scott, L. T. Fragments of Fullerenes and Carbon Nanotubes: Designed Synthesis, Unusual Reactions, and Coordination Chemistry (Wiley, Hoboken, 2012).

(22) (a) Wu, T.-C.; Hsin, H.-J.; Kuo, M.-Y.; Li, C.-H.; Wu, Y.-T. *J. Am. Chem. Soc.* **2011**, *133*, 16319. (b) Amaya, T.; Nakata, T.; Hirao, T. *J. Am. Chem. Soc.* **2009**, *131*, 10810. (c) Okuda, Y.; Fukui, N.; Kim, J.; Kim, T.; Jiang, H.-W.; Copley, G.; Kitano, M.; Kim, D.; Osuka, A. *Angew. Chem. Int. Ed.* **2017**, *56*, 12317.

(23) (a) Haddon, R. C. *J. Am. Chem. Soc.* **1987**, *109*, 1676. (b) Haddon, R. C. *Science* **1993**, *261*, 1545. (c) Haddon, R. C.; Scott, L. T. *Pure Appl. Chem.* **1986**, *58*, 137.

(24) (a) Hummelen, J. C.; Knight, B.; Pavlovich, J.; González, R.; Wudl, F. *Science* **1995**, *269*, 1554. (b) Hirsch, A.; Nuber, B. *Acc. Chem. Res.* **1999**, *32*, 795. (c) Andreoni, W.; Curioni, A.; Holczer, K.; Prassides, K.; Keshavarz-K, M. *J. Am. Chem. Soc.* **1996**, *118*, 11335. (d) Bellavia-Lund, C.; González, R.; Hummelen, J. C.; Hicks, R. G.; Sastre, A.; Wudl, F. *J. Am. Chem. Soc.* **1997**, *119*, 2946. (e) Vougioukalakis, G. C.; Orfanopoulos, M. *J. Am. Chem. Soc.* **2004**, *126*, 15956.

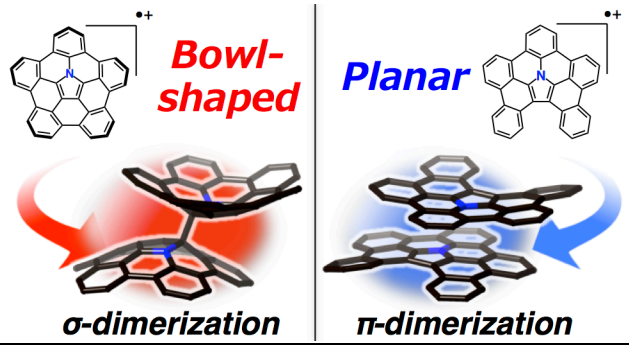
Bowl-shaped
Planar
σ-dimerization
π-dimerization